Available online at www.sciencedirect.com

SciVerse ScienceDirect

Physics Procedia 37 (2012) 891 – 898

Physics Procedia

TIPP 2011 – Technology and Instrumentation in Particle Physics 2011 June 9-14, 2011 - Chicago, Illinois, USA

Optimization of Strip Isolation for Silicon Sensors

M. Valentan[1], T. Bergauer, M. Dragicevic, M. Friedl, C. Irmler, E. Huemer, W. Treberspurg

Institute of High Energy Physics (HEPHY), Austrian Academy of Sciences, Nikolsdorfer Gasse 18, 1050 Vienna, Austria

Abstract

Precision machines like electron-positron-colliders and b-factories demand for low material budget and high position resolution when it comes to particle tracking. A low material budget can be achieved by using thin double-sided silicon detectors (DSSDs) and lightweight construction. Since thin sensors give low signals, one has to be very careful to achieve high charge collection efficiency, which requires an appropriate sensor design. In this paper we present a detailed investigation of different p-stop patterns used for strip isolation on the n-side of double-sided microstrip sensors with n-type bulk. We designed test sensors featuring the common p-stop, the atoll p-stop and a combined p-stop pattern, and for every pattern four different geometric layouts were considered. These sensors were tested at the Super Proton Synchrotron (SPS) at CERN (Geneva, Switzerland) in a 120 GeV/c hadron beam. Then they were irradiated to 700 kGy with a ^{60}Co source and subsequently tested in the same beam as before.
One geometric layout of the atoll p-stop pattern turned out to perform best, both before and after irradiation. The conclusions of these tests will be applied to the design of DSSDs for the Belle II experiment at KEK (Tsukuba, Japan).

Keywords: microstrip, silicon sensor, atoll, common, combined, p-stop, strip isolation, optimization

1. Introduction

Double-sided silicon strip detectors (DSSDs) allow two-dimensional measurements of a traversing particle's position. To make this possible, both the p-side and the n-side implantations are segmented to form strips, mostly with perpendicular orientation. Electric strip insulation is crucial to successfully operate a silicon microstrip sensor. While this is inherently given on the p-side of a DSSD, it requires additional measures on the n-side. Positive charges in the oxide attract an accumulation layer at the oxide-substrate interface, consisting of negative charge carriers. This accumulation layer shorts the n-type doped strips, unless interrupted e.g. by additional implantation of p-type doped areas, the so-called "p-stops".
In this paper we investigate different configurations of p-stop impantations and their influence on the sensor performance. We developed test sensors featuring the common p-stop, the atoll p-stop and a combined p-stop pattern, whereas for each pattern four different geometric layouts were considered.

Email address: manfred.valentan@oeaw.ac.at (M. Valentan)
[1]Corresponding author

 doi:10.1016/j.phpro.2012.04.098

2. The devices under test

The test sensors we used are small DSSDs processed by Micron Semiconductor Ltd. [1] on an n-type base material. The key parameters of the sensor and its n-side are:

- Base material: 300 μm n-type silicon, 5 kΩcm
- Full depletion voltage: 60 – 70 V
- Leakage current at full depletion: 0.43 – 0.55 μA
- Bias resistance: 40 MΩ
- Coupling capacitance: 1.13 $\frac{\mathrm{pF}}{\mathrm{cm}\,\mu\mathrm{m}}$ per strip length and width
- Number of strips: 256
- Pitch: 100 μm, no intermediate strips
- Strip implant area: 2.56 cm $\times$ 25 μm
- Strip isolation: p-stop, with varying geometry (see below)
- Strip orientation: perpendicular on p-side and n-side
- Readout: APV25 chip with analogue readout of pulse height [2] (used for the CMS [3] and Belle II experiments [4])

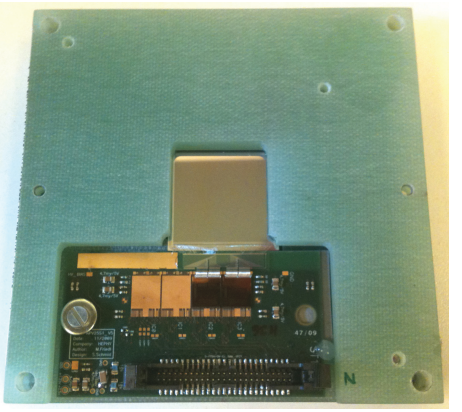

Figure 1: An uncovered test module

All sensors have been electrically characterized in the lab and proper readout has been tested with a radioactive source. The depletion voltage was determined by ramping up the reverse bias voltage while measuring the total sensor capacitance and the total leakage current. The sensor is fully depleted when both the capacitance and the leakage current reach an (almost) constant plateau.

Figure 1 shows one of the modules used in the experiment. Its top cover has been removed to reveal the sensor (center) and the readout electronics (bottom). All sensors have the same specifications and differ in the p-stop geometry only. The details of the different p-stop geometries are summarized in section 2.1.

2.1. The p-stop patterns

We used three different test sensors, each featuring a different p-stop pattern. Sketches of these patterns can be found in figure 2. N-type implantation is shown in green, p-type implantation is red.

The common pattern (figure 2(a)). The n-type doped strips are embedded in a p-type doped area covering the whole sensor. Only small regions around the strips are left unimplanted. The accumulation layer is separated and cannot short the n-type strips together. The p-stop implant itself is on the same potential all over the sensor and could therefore distribute any charge introduced in the implant. This pattern has been used for a long time and is well known.

The atoll pattern (figure 2(b)). The n-type doped strips are surrounded by isolated ringlike p-type implants. This interrupts the accumulation layer between the strips. But the accumulation layer outside the atoll implants remains intact and spreads all over the sensor. This pattern is the standard p-stop pattern nowadays.

The combined pattern (figure 2(c)). The n-type doped strips are surrounded by atoll p-stop implants. In addition, both strips and atoll implants are embedded in a p-type doped area covering the whole sensor (like in case of the common pattern). Only small regions around the strip and the atoll are left unimplanted. This pattern tries to combine the benefits of the common pattern and the atoll pattern, and was favoured by the studies [5] and [6].

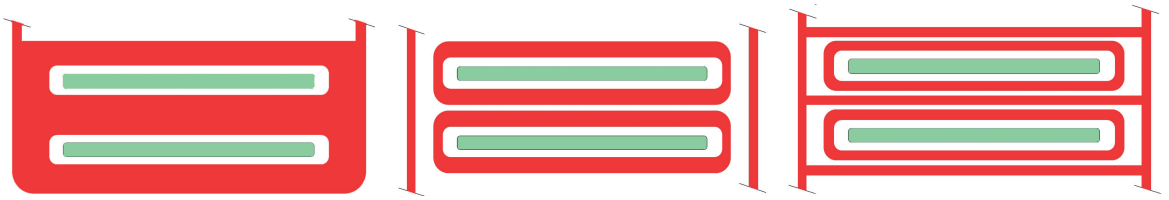

(a) The common p-stop (b) The atoll p-stop (c) The combined p-stop

Figure 2: The p-stop patterns, n-type strip implant is green, p-stop implant is red. (Drawings taken from [5])

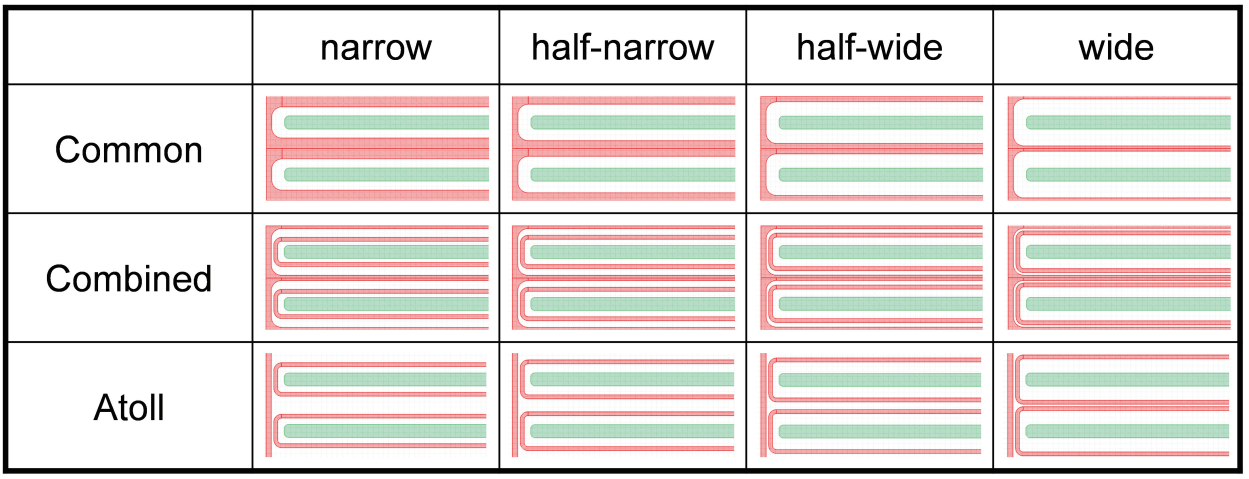

Figure 3: The different p-stop patterns and geometries. Green: n-type implants (strips); red: p-stop implants

2.2. *The geometry of the p-stop patterns*

There are four zones on each sensor, differing by the geometry of the p-stop pattern, where each zone consists of 64 strips. So, in total we compare twelve different p-stop geometries. For each pattern, the distance between the n-type strip implant and the p-stop implant is varied. Hence the geometries are named “narrow”, “half-narrow”, “half-wide” and “wide”, where for the “narrow” geometry the p-stop implant is close to the strip, and for the “wide” geometry it is far away. Figure 3 shows details of these designs.

Details of the geometries can be found in table 1. Here, “atoll width” denotes the width of the ring-like p-type implant. “Bar width” denotes the width of the p-type implant part of the common structure, which is between the strips. “Distance” denotes the width of the unimplanted region between strip implant and p-stop implant. These dimensions are shown in figure 4.

		narrow	half-narrow	half-wide	wide
Common	bar width (bw)	40	30	20	10
	distance (d)	17.5	22.5	27.5	32.5
Combined	bar width (bw)	10	10	10	10
	atoll width (aw)	7.5	7.5	7.5	7.5
	distance (d)	8	12	16	20
Atoll	atoll width (aw)	7.5	7.5	7.5	7.5
	distance (d)	12.5	17.5	22.5	27.5

Table 1: The dimensions of the different p-stop geometries, values are given in μm

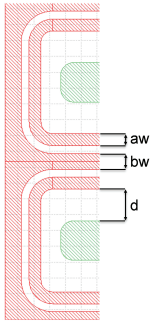

Figure 4: Geometry with dimensions

3. The experimental setup

The sensors described in section 2 were tested in a hadron beam at CERN, then taken to SCK•CEN [7] for γ-irradiation, and afterwards tested in the same setup as before, again at CERN. This was done within a period of two weeks in October 2010.

3.1. The beam test at CERN

The beam test took place at the H6 beam line of the SPS (Super Proton Synchrotron), located at the Prévessin site of CERN. This beam line was configured to provide 120 GeV/c hadrons, most of which were pions.
The sensors were placed on the beam together and a reverse bias voltage of 100 V was applied. We acquired 100k events, both before and after irradiation.

3.2. The irradiation at SCK•CEN

The irradiation took place at SCK•CEN in Mol, Belgium. This facility provides an underwater ^{60}Co gamma source with a dose rate of 25 kGy/h. We irradiated the sensors to 700 kGy, while the accumulated lifetime dose of the Belle II experiment is expected to be less than 100 kGy.

4. Definition of the measured quantities

We measure the detector performance in terms of the signal-to-noise-ratio (SNR), which is one of the main contributions to the position accuracy. The SNR for a cluster[2] consisting of n strips reads

$$SNR_n = \frac{S_{\text{cluster}}}{N_{\text{cluster}}} = \frac{\Sigma_{i=1}^{n} S_i}{\sqrt{\Sigma_{i=1}^{n} N_i^2}}, \tag{1}$$

where S_i and N_i denote the signal and the noise of strip i, respectively. In the analysis, we only consider events that created a cluster of exactly two strips, because for these events the effects of charge sharing is clearly visible. Events with only one hit strip do not share charge and are therefore not sensitive to the p-stop between the strips. For clusters consisting of two strips the SNR is reduced to

$$SNR_{n=2} = \frac{S_1 + S_2}{\sqrt{N_1^2 + N_2^2}}. \tag{2}$$

4.1. Cluster signal

The APV25 chip is capable of taking multiple samples of the shaped waveform when readout is triggered. For determining the peak signal and the precise hit time, six samples around the signal peak are recorded. The cluster signal for each sample is calculated by summation of the respective samples of all adjacent strips above a certain threshold and therefore contributing to the cluster. Note that this procedure yields the cluster signal and not the single strip signal. Then these samples are fitted with a reference waveform to obtain amplitude and timing (see figure 5). The reference waveform is taken from an internal calibration scan of the APV25 chip [8]. The cluster signal values obtained by this procedure follow a Landau distribution with a small admixture of a normal distribution. The Landau distribution describes the distribution

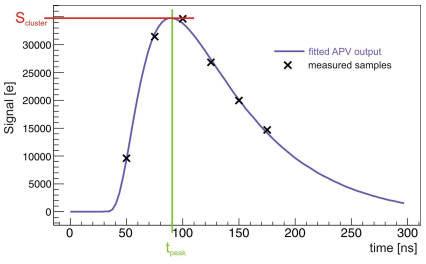

Figure 5: Definition of the cluster signal

[2]Cluster: two or more adjacent strips with signals above a certain threshold. The signal of the seed strip is required to be five times as high as the strip noise, for the neighbouring strips signals three times as high as the respective strip noises are required. The total cluster signal has to be at least five times as high as the total cluster noise.

of energy deposition by ionization, whereas the Gaussian part accounts for electronic noise and fluctuations of the charge cloud by diffusion. We fit a convolution of a Landau probability density function (pdf) with a normal pdf to a histogram of the cluster signal values. The free parameters of the fit are the most probable value and the width of the Landau pdf, as well as the width of the Gaussian pdf and the amplitude of the overall (convoluted) pdf. Both distributions are equally normalized to each other, i.e. with a relative normalization of 1. For comparisons of signal yield we use the most probable value given by this fit.

4.2. Strip noise and cluster noise

At the start of each data taking run, we take 600 readings with random triggers and no beam. This ensures that the sensor does not give a signal at the time of the trigger. The pedestal offset of the individual strips is calculated as the mean value of the first 200 readings of each strip, which is hereafter substracted from all following readings. For each one of the next 200 readings the mean value of blocks of 32 strips is calculated, which gives the common mode noise of the considered reading. For each strip a first approximate noise value is calculated as the root mean square (RMS) value of these 200 readings, after subtracting from each reading the respective common mode noise. From now on, strips with a high value of this approximate noise are omitted when calculating common mode noise. Finally, the last 200 readings are histogrammed for each strip after pedestal subtraction and common mode correction, and the resulting distribution is fitted with a Gaussian function. The standard deviation of this Gaussian is the single strip noise, whereas the cluster noise is hereafter calculated according to the denominator in equation 1.

4.3. Signal-to-noise ratio

The SNR is calculated according to equation 1, where the cluster signal and the strip noise are defined in sections 4.1 and 4.2, respectively. Like the cluster signal values, also the SNR values follow a Landau distribution with a small admixture of a normal distribution. An eventual improper sensor design would lower the cluster signal, and it would raise the cluster noise. Both effects translate into a shift of the peak of the SNR distribution. That's why we are not interested in the width of the SNR distribution, but only in its most probable value. We fit a convolution of a Landau pdf with a normal pdf to a histogram of the SNR values. The fit parameters are again the most probable value and width of the Landau pdf, the width of the Gaussian pdf and the amplitude. For comparing the detector performance we use the fit results for the most probable value (MPV) of the distribution. All possible fluctuations that would widen the Gaussian part of the distribution are irrelevant for the comparison, because they don't affect the average behaviour of the sensor, i.e. the most probable SNR.

4.4. Calibration of the signal measurement

When triggered, the readout system reads the levels of its input channels in ADC counts. One has to perform a calibration to match these numbers to the physical signal charge. The readout chip injects a calibration pulse on selected strips and measures the system response, which is then used to calculate the number of electrons per ADC count. The calibration pulse nominally corresponds to an injected charge of 22500 electrons [8].

This calibration procedure has to deal with some sources of inaccuracy. The height of the calibration pulse can differ from chip to chip, moreover the system response to the calibration pulse can change from channel to channel due to small differences of the charge injection capacitors and the preamplifiers. Both effects influence the calibrated value of the cluster signal and of the strip noise. The uncertainties of the charge injection capacitors do not carry much weight for the final most probable cluster signal values, because the MPV values represent an average over many input channels. However, the amplitude of the calibration pulse applies to the chip as a whole and does change the most probable value of the signal. In contrast, for the signal-to-noise ratio all these effects cancel out on a strip-by-strip basis, making the results comparable.

So, the choice of the SNR for our comparison is not only a practical one. We compare the sensor behaviour both before and after the irradiation, where both the sensors and the readout electronics are irradiated. The irradiation not only changes the sensor behaviour, but may also affect the gain (and thus calibration) of the readout electronics. The latter effect cancels out for the SNR, so that its values both before and after irradiation can be directly compared.

5. Results

5.1. Comparison of the cluster signal

Figures 6(a) and 7(a) show the most probable cluster signal of all p-stop geometries for clusters of exactly two strips, where the values found in figure 6(a) are before irradiation and those in figure 7(a) are after irradiation. We observe that in the unirradiated case the most probable cluster signal of the combined and atoll p-stop geometries are comparable and show little dependence on the geometry dimensions, while for the common p-stop the signal changes significantly with the geometry. In general, a part of the signal is lost when electric field lines do not arrive at the strip implant [6]. For the common p-stop pattern the total p-implanted area differs depending on the geometry, pushing the field lines towards the strip implant, while for the other p-stop patterns a change in the geometry opens up unimplanted regions between the p-stop implants where field lines can end up. This qualitatively explains the geometry dependence of the cluster signal.

After irradiation the common p-stop shows a very equalized and high cluster signal for all geometries, while the other ones show a clear tendency for higher cluster signals when going to the wide geometry. The highest cluster signal is found for the wide atoll p-stop.

Due to uncertainties of the calibration one has to be careful when comparing the absolute values of the signals. Each p-stop pattern resides on a different sensor, and each sensor is read out by two APV25 chips. Strictly speaking one can only compare p-stop geometries read out by the same chip, i.e. the wide and half-wide geometries and the narrow and half-narrow geometries separately. One can *not* directly compare narrow and wide geometries, nor different p-stop patterns. Especially values before and after irradiation can not be compared due to different readout chip settings. For a direct comparison consider the SNR *only*!

5.2. Comparison of the cluster noise

Figures 6(b) and 7(b) show, for each of the p-stop geometries, the average cluster noise for clusters of exactly two strips $\bar{N}_{n=2} = \sqrt{2}\bar{N}_{\text{strip}}$, where $\bar{N}_{\text{strip}}$ is the noise averaged over all strips of the same group. Again, figure 6(b) is before irradiation and figure 7(b) is after irradiation. We observe that in the unirradiated case the average cluster noise gets better when increasing the distance between strip implant and p-stop implant, i.e. going to the wide geometries. Here, the common and combined p-stop geometries behave similarly, while the atoll p-stop performs slightly better, by a factor of about 10%. After irradiation the combined p-stop suffers strongly, while again the atoll p-stop shows the lowest cluster noise. Again, for comparison of noise levels the same restrictions apply as for the cluster signal levels!

5.3. Comparison of the cluster signal-to-noise ratio

Figures 6(c) and 7(c) show the SNR for clusters[3] of exactly two strips before and after irradiation. The effect of the different calibrations cancels out for the SNR – even between measurements taken before and after irradiation – so that we can compare the values directly.

Before irradiation (figure 6(c)) the half-wide atoll p-stop clearly beats all other options. This is due to a decent signal height and a very low noise. For the common p-stop the high signals of the narrow geometries are counteracted by high noise levels, causing it to fall back behind the atoll p-stop for all geometries. The combined p-stop shows high signal levels for the wide geometries, but also higher noise levels. This leads to the best SNR for the wide geometry, for all other geometries it is surpassed by the atoll p-stop (and also by the common p-stop).

After irradiation (figure 7(c)) the atoll p-stop performs best for the wide geometries, again reaching the best SNR for the half-wide geometry. This is mainly due to very high signal levels and low noise compared to the other patterns. The common pattern beats the other patterns for the narrow geometries, where it shows high signals and low noise on its part. Compared to the other patterns, the combined pattern loses some signal while its noise is larger by almost 30% after irradiation, so its SNR suffers strongly from irradiation.

Figure 8 shows the most probable SNR value for each of the p-stop geometries, with the unirradiated and irradiated SNR values plotted side-by-side. Here one can directly see the drop of the SNR after irradiation, which is severe for the combined p-stop.

[3] Note that the computation of the cluster signal-to-noise ratio uses the individual strip noise values of the strips involved in the cluster, according to the definition in equation 2, and not the averaged cluster noise displayed in figures 6(b) and 7(b).

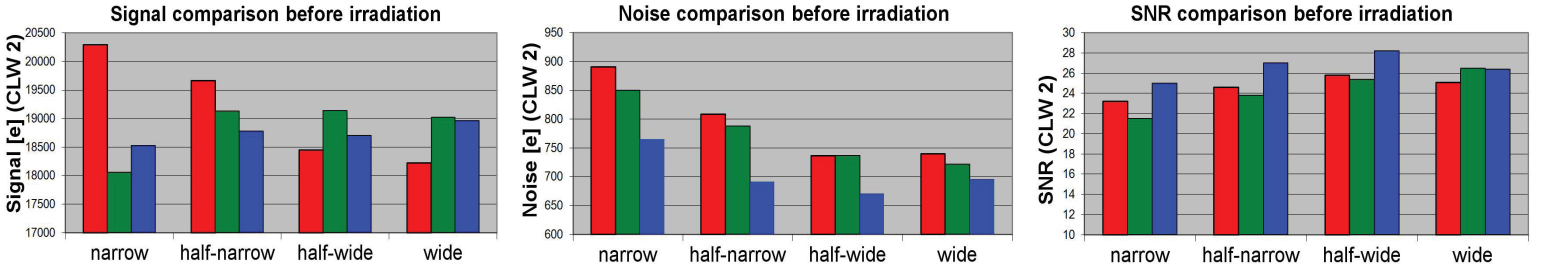

(a) Cluster signal comparison – unirradiated (b) Cluster noise comparison – unirradiated (c) Cluster SNR comparison – unirradiated

Figure 6: Comparison of cluster signal, cluster noise and cluster SNR before irradiation. Red: common p-stop, green: combined p-stop, blue: atoll p-stop

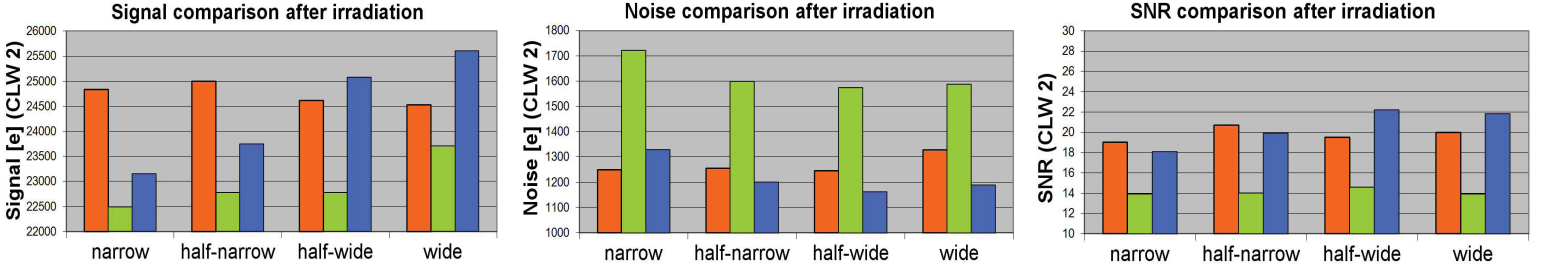

(a) Cluster signal comparison – irradiated (b) Cluster noise comparison – irradiated (c) Cluster SNR comparison – irradiated

Figure 7: Comparison of cluster signal, cluster noise and cluster SNR after irradiation. Orange: common p-stop, light green: combined p-stop, light blue: atoll p-stop

(a) Common p-stop geometries (b) Combined p-stop geometries (c) Atoll p-stop geometries

Figure 8: Comparison of cluster SNR per p-stop pattern. Dark colors are before irradiation, light colors are after irradiation

The SNR diagrams contain no error bars because the uncertainty of the most probable value's (MPV) fit result is too small to be displayed. Since we compare the fit value of the MPV, the uncertainty of the fit result is relevant for the comparison, and not the width of the Landau distribution. The uncertainty values can be found in table 2, at the end of this section.

Summing up, the half-wide atoll pattern showed the best performance of all geometries, both before and after irradiation. The exact SNR values including fit uncertainties are summarized in table 2.

		narrow	half-narrow	half-wide	wide
Common	unirradiated	23.2 ± 0.08	24.6 ± 0.07	25.8 ± 0.07	25.1 ± 0.06
	irradiated	19.0 ± 0.06	20.7 ± 0.05	19.5 ± 0.05	20.0 ± 0.04
Combined	unirradiated	21.5 ± 0.06	23.8 ± 0.06	25.4 ± 0.07	26.5 ± 0.08
	irradiated	13.9 ± 0.02	14.0 ± 0.03	14.6 ± 0.03	13.9 ± 0.04
Atoll	unirradiated	25.0 ± 0.06	27.0 ± 0.07	28.2 ± 0.08	26.4 ± 0.06
	irradiated	18.1 ± 0.03	19.9 ± 0.04	22.2 ± 0.04	21.8 ± 0.04

Table 2: Most probable SNR fit values of the p-stop patterns and geometries. Green: best value within one pattern; Red: overall best value.

The fraction of 2-strip-clusters w.r.t. 1-strip-clusters is in the order of 0.4 for the common and combined p-stop patterns, whereas for the atoll p-stop pattern it reaches about 0.8. This also displays that charge sharing is better for the atoll p-stop pattern.

6. Summary and outlook

We designed and tested double sided n-substrate test sensors (100 μm pitch on the n-side, no intermediate strips) featuring the common p-stop pattern, the atoll p-stop pattern, and a combined p-stop pattern, with four geometric variants of each pattern. These sensors were tested in a 120 GeV/c hadron beam before and after irradiation to 700 kGy with ^{60}Co gammas. In the analysis we only considered events forming clusters of exactly two strips. The best performing p-stop geometry (in terms of SNR) turned out to be the half wide atoll pattern, which outperforms all other variants both before and after irradiation. This is due to a high signal level and the lowest noise observed in all variants. A simulation study is ongoing in order to explain the experimental findings on a microscopic level.

Since the Belle II experiment will use sensors with one intermediate strip both on the p-side and on the n-side, we will extend the measurements by investigating the performance of the same sensors with only every second strip connected to the readout electronics. This allows to study the behaviour of a sensor with a pitch of 200 μm and one intermediate strip. Moreover, we will investigate sensors featuring the p-spray strip separation technique, with and without intermediate strips in the near future. The conclusions of the presented and following tests will be applied to the design of DSSDs for the Silicon Vertex Detector (SVD [9]) of the Belle II experiment [4] at KEK [10].

References

[1] Micron Semiconductor Limited (Lancing, Sussex, England), http://www.micronsemiconductor.co.uk/.
[2] M. French et al., Design and results from the APV25, a deep sub-micron CMOS front-end chip for the CMS tracker, Nucl. Instr. and Meth. A 466 (2001) 359–365.
[3] T.S. Virdee (CMS Collaboration), The CMS Experiment at the LHC, http://cmsdoc.cern.ch/cgi-doc/Grep/documents/all.html? GEN.
[4] Z. Doležal, S. Uno (editors), Belle II Technical design report, KEK Report 2010-1, arXiv:1011.0352v1 [physics.ins-det], 2010.
[5] Y. Unno et al., Evaluation of P-stop Structures in the N-side of N-on-N Silicon Strip Detector, IEEE Transactions On Nuclear Science 45 (1998) 401–405.
[6] Y. Iwata et al., Optimal P-Stop Pattern for the N-Side Strip Isolation of Silicon Microstrip Detectors, IEEE Transactions On Nuclear Science 45 (1998) 303–309.
[7] SCK•CEN: Dutch: Studiecentrum voor Kernenergie, French: Centre d'Étude de l'énergie Nucléaire (Mol, Belgium), http://www.sckcen.be/.
[8] L. Jones et al., APV25-S1 User Guide, Version 2.2.
[9] M. Friedl et al., The Belle II Silicon Vertex Detector, this volume.
[10] KEK – High Energy Accelerator Research Organization (Tsukuba, Ibaraki, Japan), http://www.kek.jp.